Metabolic Brain Disease (2019) 34:223–233
https://doi.org/10.1007/s11011-018-0345-9

ORIGINAL ARTICLE

Differential regional infarction, neuronal loss and gliosis in the gerbil cerebral hemisphere following 30 min of unilateral common carotid artery occlusion

Ji Hyeon Ahn[1] · Minah Song[2] · Hyunjung Kim[2] · Tae-Kyeong Lee[2] · Cheol Woo Park[2] · Young Eun Park[2] · Jae-Chul Lee[2] · Jun Hwi Cho[3] · Young-Myeong Kim[4] · In Koo Hwang[5] · Moo-Ho Won[2] · Joon Ha Park[1]

Received: 7 August 2018 / Accepted: 12 November 2018 / Published online: 15 November 2018

Abstract

The degree of transient ischemic damage in the cerebral hemisphere is different according to duration of transient ischemia and cerebral regions. Mongolian gerbils show various lesions in the hemisphere after transient unilateral occlusion of the common carotid artery (UOCCA) because they have different types of patterns of anterior and posterior communicating arteries. We examined differential regional damage in the ipsilateral hemisphere of the gerbil after 30 min of UOCCA by using 2,3,5-triphenyltetrazolium chloride (TTC) staining, cresyl violet (CV) Nissl staining, Fluoro-Jade B (F-J B) fluorescence staining, and NeuN immunohistochemistry 5 days after UOCCA. In addition, regional differences in reactions of astrocytes and microglia were examined using GFAP and Iba-1 immunohistochemistry. After right UOCCA, neurological signs were assessed to define ischemic symptomatic animals. Moderate symptomatic gerbils showed several infarcts, while mild symptomatic gerbils showed selective neuronal death/loss in the primary motor and sensory cortex, striatum, thalamus, and hippocampus 5 days after UOCCA. In the areas, morphologically changed GFAP immunoreactive astrocytes and Iba-1 immunoreactive microglia were found, and their numbers were increased or decreased according to the damaged areas. In brief, our results demonstrate that 30 min of UOCCA in gerbils produced infarcts or selective neuronal death depending on ischemic severity in the ipsilateral cerebral cortex, striatum, thalamus and hippocampus, showing that astrocytes and microglia were differently reacted 5 days after UOCCA. Taken together, a gerbil model of 30 min of UOCCA can be used to study mechanisms of infarction and/or regional selective neuronal death/loss as well as neurological dysfunction following UOCCA.

Keywords Astrocytes · Fluoro Jade B · Gerbil · Microglia · Selective neuronal death · Transient focal ischemia

Introduction

Most of animal models for transient focal brain ischemia have been developed by the occlusion of middle cerebral artery (Canazza et al. 2014). Therefore, transient focal brain ischemia in experimental animals is highly reproducible and has been widely used due to low mortality rate (Katchanov et al. 2003; Sicard and

Ji Hyeon Ahn and Minah Song contributed equally to this article.

✉ Moo-Ho Won
mhwon@kangwon.ac.kr

✉ Joon Ha Park
jh-park@hallym.ac.kr

[1] Department of Biomedical Science and Research Institute for Bioscience and Biotechnology, Hallym University, Chuncheon, Gangwon 24252, Republic of Korea

[2] Department of Neurobiology, School of Medicine, Kangwon National University, Chuncheon, Gangwon 24341, Republic of Korea

[3] Department of Emergency Medicine, and Institute of Medical Sciences, Kangwon National University Hospital, School of Medicine, Kangwon National University, Chuncheon 24341, Gangwon, Republic of Korea

[4] Department of Molecular and Cellular Biochemistry, School of Medicine, Kangwon National University, Chuncheon 24341, Gangwon, Republic of Korea

[5] Department of Anatomy and Cell Biology, College of Veterinary Medicine, and Research Institute for Veterinary Science, Seoul National University, Seoul 08826, Republic of Korea

Fisher 2009). Many researchers need much more damaged area in brains to study differential neuronal damage and its mechanisms and have used a gerbil model of unilateral occlusion of the common carotid artery (UOCCA) to produce hemispheric ischemic damage, which means an experimental broad focal cerebral ischemia, particularly to induce cortical ischemia (Hanyu et al. 1997; Hanyu et al. 1993; Ito et al. 2014). Relative simplicity of the operation procedure in gerbils compared to rats or mice is the biggest advantage of this model due to lack of the posterior communicating arteries (Murakami et al. 1998). In addition, the gerbil model of bilateral occlusion of the common carotid arteries is the best in long observation after ischemia because the brainstem is not damaged (Levy et al. 1975) and survive long time (Lee et al. 2016a). Despite these advantages, this gerbil model has shown disadvantages that the extent of the hemispheric ischemic damage varies due to different types of patterns of anterior and posterior communicating arteries (Du et al. 2011). In this regard, it is of fundamental importance to identify the extent of damaged area (infarct) and the degree of the damage in the hemisphere induced by UOCCA in gerbils to investigate characteristics of neuronal degeneration and neurological pathophysiology in the gerbils. Some studies have proven valid methods in a gerbil model of UOCCA, such as the assessment of neurological behavior (Ohno et al. 1984), the examination of the diameter and appearance of the common carotid artery after temporary occlusion (Matsumoto et al. 1988), and the observation of the retinal arterial perfusion by ophthalmoscopy (Oostveen et al. 1992), which are correlated with histopathological results in the ischemic hemisphere after UOCCA.

It is well known that focal ischemia produces two fundamentally different types of morphological damage, selective neuronal loss and infarction, depending on the intensity of the ischemic insult (the duration or frequency of ischemia) (Hanyu et al. 1997; Hanyu et al. 1995). In particular, ischemic damage in some regions shows different vulnerability after transient ischemia. For example, selective neuronal loss/death occurs in CA1 area, not CA2 and 3 areas, in the hippocampus induced by 5 min of transient ischemia (Kirino and Sano 1984), in layer III, V, and VI in the somatosensory cortex induced by 5 to 15 min of transient ischemia (Lee et al. 2013), and in the dorsolateral field in the striatum induced by 30 min of transient ischemia (Park et al. 2018).

Some researchers have examined ischemic damage in the hemisphere of the gerbil brain after permanent UOCCA (Rodriguez Cruz et al. 2010) or repeated transient UOCCA (Ishibashi et al. 2003). However, few studies using a single transient UOCCA have been fully investigated. Therefore, the purpose of this study was to investigate the severity of neuronal damage using Fluoro-Jade B (F-J B), which is a reliable maker for neuronal degeneration (Schmued et al. 1997) as well as gliosis (astrocytosis and microgliosis) using immunohistochemistry in various brain regions of the hemisphere following a 30 min of UOCCA in gerbils.

Materials and Methods

Experimental animals

Male Mongolian gerbils (total n = 66) were obtained at 6 months of age (body weight, 70-75 g) from the Experimental Animal Center (Kangwon University, Chuncheon, Gangwon, Republic of Korea) and kept at a constant temperature (23°C) and humidity (50%) with a 12-h light/dark cycle. The process of the care and handling of the gerbils conformed to the guidelines following current international laws and policies (NIH Guide for the Care and Use of Laboratory Animals, The National Academies Press, 8th Ed., 2011). The protocol of this experiment was approved by the Institutional Animal Care and Use Committee (IACUC) at Kangwon National University (approval no. KW-180124-1).

Induction of UOCCA

As previously described (Ishibashi et al. 2004), in brief, the gerbils were anesthetized with a mixture of 2.5% isoflurane (Baxtor, Deerfield, IL) in 33% oxygen and 67% nitrous oxide. UOCCA was carried out at right side for 30 min using non-traumatic aneurysm clips after a midline incision on the ventral surface of the neck. The normal body (rectal) temperature (37 ± 0.5°C) was regulated using a thermometric blanket and monitored with a rectal temperature probe (TR-100; Fine Science Tools, Foster City, CA).

Groups according to neurological scores

After UOCCA surgery, neurological signs of the animals were observed two times at 15 min and 30 min after UOCCA, according to a previously reported method for quick evaluation of six neurological signs (Matsumoto et al. 1988). In brief, 1) disturbance of consciousness (drowsiness; paucity

Table 1 The number of animals and survival rate at 5 days after UOCCA according to neurological symptoms

Class (group)	Severe	Moderate	Mild	None
Neurologic score	6 to 7	3 to 5	1 to 2	0
Numbers	6 (9.1 %)	10 (15.2 %)	21 (31.8 %)	29 (43.9 %)
Survival rate (%)	0	100	100	100

of movement, semicoma; no movement but preserved righting reflex, and coma; loss of righting reflex), 2) contralateral hemiparesis, 3) ipsilateral circling, 4) contralateral ptosis, 5) torsion of the neck and 6) seizure were chosen, and each sign was scored as 1 point, semicoma and seizure were scored 2 points, and the maximal score of 7 was automatically given when coma occurred. Based on the neurological score (the mean value of each neurological test), the ischemic gerbils were divided into four groups, as shown in Table 1: severe (score 6-7) group (n=6), moderate (score 3-5) group (n=10), mild (score 1-2) group (n=21), and none (score 0) group (n=29).

Staining of infarcts

To identify distribution of ischemic infarcts in the whole brain, 2,3,5-triphenyltetrazoliumchloride (TTC) staining was performed according to our published procedure (Ha Park et al. 2016). In brief, the ischemic gerbils were anesthetized with 60 mg/kg pentobarbital sodium (JW Pharm. Co., Ltd., Korea) and euthanized by rapid cervical dislocation 5 days after UOCCA. Brains in each group (n=5 in moderate, mild and none group) were removed, and six coronal slices (1 mm thickness) were made using a gerbil brain slicer (ASI Instruments, Inc., MI, USA). The slices were immersed immediately in a 2% 2,3,5-TTC solution (Sigma-Aldrich, St. Louis, Missouri) at 37°C for 20 min. The TTC-stained brain tissues were fixed in 4% phosphate-buffered formalin and photographed in color using a digital camera.

Tissue preparation for histology

For histology in the cerebral cortex, striatum, thalamus and hippocampus, we used the none and mild group (n = 7 in each group) at 5 days after UOCCA; we did not examine the moderate group because the group had infarcts, which are necrotic tissues and do not show selective neuronal death/loss. The animals were anesthetized with 30 mg/kg Zoletil 50 (Virbac, Carros, France) and perfused transcardially with 0.1 m phosphate buffered saline (PBS, pH 7.4) followed by 4% paraformaldehyde in 0.1 m phosphate buffer (PB, pH 7.4). The brains were cryoprotected and serially sectioned into 30-μm coronal sections in a cryostat (Leica, Wetzlar, Germany).

Cresyl violet (CV) staining

To investigate cellular morphology, CV staining was performed according to our published protocol (Ahn et al. 2016). In brief, CV acetate (Sigma, MO) was dissolved at 1.0% (w/v) in distilled water, and glacial acetic acid was added to this solution. The sections were mounted on gelatin-coated microscopy slides, stained with CV and dehydrated by immersing in serial ethanol baths. Finally, the stained sections were covered with Canada balsam (Kanto, Tokyo, Japan).

Fluoro-Jade (F-J) B histofluorescence staining

To investigate the degeneration/death of cells, F-J B (a fluorescent marker for the localization of cellular degeneration) histofluorescence staining was conducted according to the method published by Candelario-Jalil et al. (Candelario-Jalil et al. 2003). In brief, the sections were first immersed in a solution containing 1% sodium hydroxide in 80% alcohol and followed in 70% alcohol. They were then transferred to a solution of 0.06% potassium permanganate, and to a 0.0004% F-J B (Histochem, Jefferson, AR) staining solution. After washing them, they were placed on a slide warmer (approximately 50°C) to be reacted. The reacted sections were examined using an epifluorescent microscope (Carl Zeiss, Germany) with blue (450–490 nm) excitation light and a barrier filter.

Immunohistochemistry

To examine the morphology and distribution of neurons, astrocytes, and microglia, immunohistochemistry was done according to our published method (Lee et al. 2016b). In short, the sections were sequentially treated with 0.3% hydrogen peroxide (H_2O_2) in PBS for 30 min and 10% normal donkey serum in 0.05 M PBS for 30 min. The treated sections were incubated with the primary antibodies; mouse anti-NeuN (1:1,000, Chemicon, Temecula, CA), mouse anti-GFAP (1:800, Abcam), and rabbit anti-Iba-1 (1:800, Wako) overnight at 4°C. The incubated sections were exposed to biotinylated goat anti-mouse or goat anti-rabbit IgG (1:200, Vector, Burlingame, CA) and streptavidin peroxidase complex (1:200, Vector). Finally, the reacted sections were visualized by staining with 3, 3'-diaminobenzidine tetrahydrochloride in 0.1 M Tris–HCl buffer (pH 7.2). In order to establish the specificity of each immunostaining, a negative control test was carried out with pre-immune serum instead of each primary antibody. The negative control resulted in the absence of immunoreactivity in any structures (data not shown).

Data analysis

We analyzed numbers of F-J B, NeuN, GFAP, and Iba-1 positive cells according to our published method (Bae et al. 2015). In brief, we selected five sections from each animal with 120-μm interval according to anatomical landmarks corresponding to antero-posterior +1.5 to −0.1 mm for the cortex and striatum, and −1.65 to −2.7 mm for the thalamus and hippocampus of the gerbil brain atlas (Radtke-Schuller et al. 2016). Images of NeuN and F-J B positive cells in the cortex (the primary motor and sensory cortex), striatum, and

thalamus and hippocampus were captured by using an AxioM1 light microscope (Carl Zeiss, Göttingen, Germany) equipped with a digital camera (Axiocam, Carl Zeiss) connected to a PC monitor. Positive cells were obtained in a 250 × 250 μm square, and cell counts were obtained by averaging the total number of F-J B, NeuN, GFAP, and Iba-1 positive cells from each animal per group by using an Adobe Photoshop version 8.0 and analyzed using Image J 1.46 software (National Institutes of Health, Bethesda, MD).

Statistical analysis

The data shown here represent the means ± SEM. Differences of the means among the groups were statistically analyzed by analysis of variance (ANOVA) with Duncan's post hoc test using SPSS 17.0 software (IBM, New York, USA). Statistical significance was considered at $P < 0.05$.

Results

Infarcts by TTC staining

In the asymptomatic gerbils, no obtrusive ischemic infarcts were found in the ischemic hemisphere induced by 30 min of UOCCA when we stained the hemisphere by using TTC staining (Fig. 1). In the mild symptomatic gerbils, ischemic lesions detected by TTC staining were palely distributed in the parietal cortex, the dorsolateral field of the striatum (caudate putamen), and the field CA1-3 of the hippocampus (hippocampus proper) of the ischemic hemisphere 5 days after UOCCA (Fig. 1). In the moderate symptomatic gerbils, distinct infarcts were shown in the frontoparietal cortex (the forelimb field of primary somatosensory cortex), the parietal cortex (the barrel field of primary somatosensory cortex), the primary visual cortex, the primary auditory cortex, the dorsolateral field of the striatum, the thalamus, and the hippocampus (hippocampus proper) in the ischemic hemisphere 5 days after UOCCA.

CV positive cells

As described in the Methods section, we examined selective neuronal death/loss in the mild gerbils (Fig. 1). In the cerebral cortex of the contralateral (non-ischemic) hemisphere of the mild gerbils as well as the normal gerbils, normal CV positive cells were easily found throughout six cortical layers in the primary motor (M1) and sensory (S1) cortex, and large CV positive cells, of which diameter was larger than 10 μm, showed a pale nucleus and dark cytoplasm (Fig. 2 A-A2, C-C2). However, in the ipsilateral M1 and S1 cortex, CV positive cells in layer II-III (Fig. 2 B-B2) and V-VI (Fig. 2 D-D2) showed pale cytoplasm due to loss of Nissl substance, and they were distinctively decreased in numbers compared to those in the contralateral cortex 5 days after UOCCA.

In the striatum, many large cells in the contralateral and normal striatum were well stained with CV throughout the striatum (Fig. 2 E, E1). In contrast, CV-positive cells in the dorsolateral field of the ischemic striatum were considerably decreased in numbers 5 days after UOCCA (Fig. 2 F, F1).

In the thalamus, large CV positive cells were rarely shown in the contralateral thalamus (Fig. 2 G, G1), although many large CV positive cells were distributed in the ipsilateral thalamus 5 days after UOCCA (Fig. 2 H, H1).

In the hippocampus, CV positive cells in the contralateral hippocampus were mainly observed in the stratum pyramidale (SP) of the CA1-3 field (Fig. 2 I1, I2) and in the granular cell layer (GCL) of the dentate gyrus (Fig. 2 I3). However, in the ipsilateral hippocampus, a significant loss of CV positive cells was found in the SP of the CA1-3 field (Fig. 2 J1, J2), and in the polymorphic layer (PL) of the dentate gyrus (Fig. 2 J3) 5 days after UOCCA.

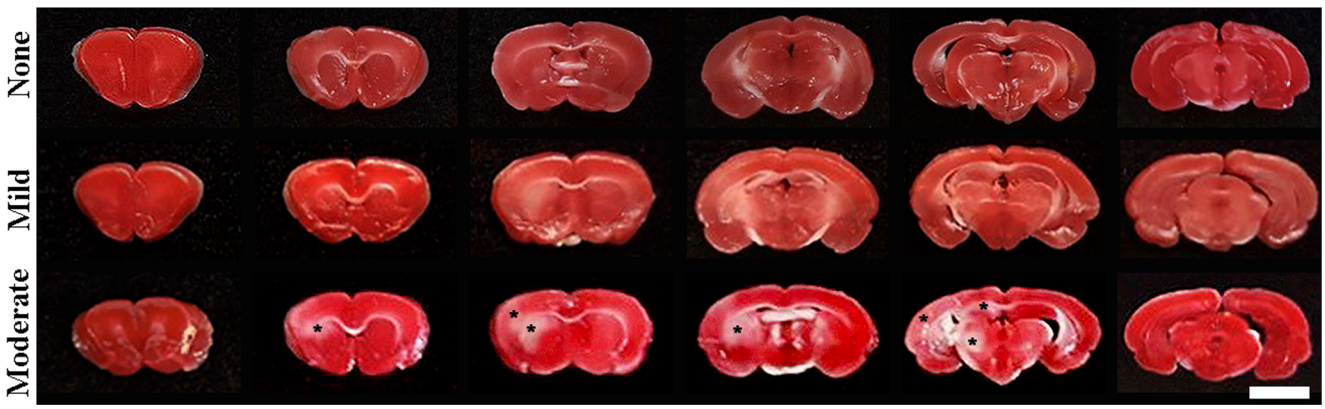

Fig. 1 TTC staining in the brain sections of the none (top low), mild (middle low), and moderate (bottom low) group 5 days after UOCCA. Core regions of infarcts are indicated (asterisks) in the parietal cortex, striatum, thalamus, and hippocampus of the ipsilateral hemisphere of the moderate group, whereas no obvious infarcts were found in the mild group. The left side of each brain slice is the ipsilateral (ischemic) hemisphere. (n = 5) Scale bar: 5000 μm

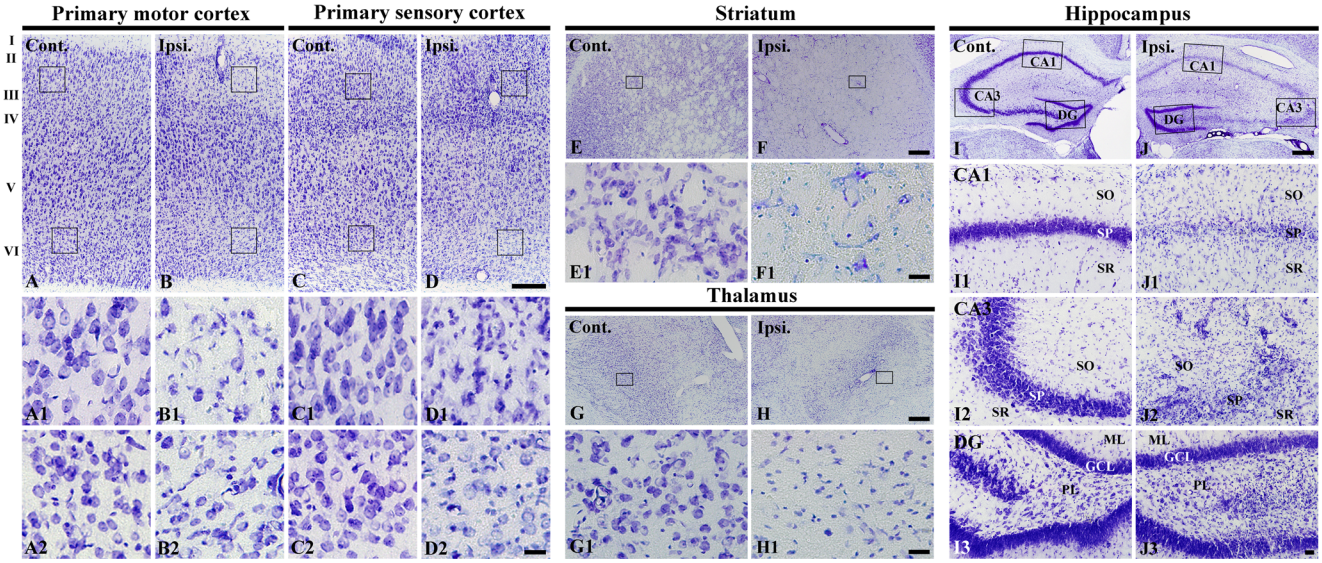

Fig. 2 CV staining in the M1 (**a**, **b**) and S1(**c**, **d**) cortex, striatum (**e**, **f**), thalamus (**g**, **h**), and hippocampus (**i**, **j**) of the contralateral (**a**, **c**, **e**, **g**, **i**) and ipsilateral (**b**, **d**, **f**, **h**, **j**) hemisphere of the mild group 5 days after UOCCA. In the ipsilateral hemisphere, CV positive cells are apparently decreased in the M1 and S1 cortex, striatum, thalamus, and hippocampus compared to those in the contralateral hemisphere. GCL, granular cell layer; ML, molecular layer; PL, polymorphic layer; SO, stratum oriens; SP, stratum pyramidale; SR, stratum radiatum. Scale bars: A-J = 200 μm, A1-J3 = 25 μm

F-J B positive cells

In the M1 and S1 cortex in the contralateral hemisphere, no F-J B positive cells were found in any cortical layers (Fig. 3 A-A2, C-C2). However, many F-J B positive degenerating cells were detected in layers II-III (Fig. 3 B-B2) and V-VI (Fig. 3 D-D2) of the ipsilateral M1 and S1 cortex 5 days after UOCCA (Fig. 3K).

In the striatum, F-J B positive cells were not shown in the contralateral side (Fig. 3 E, E1). However, many F-J B positive cells were found in the ipsilateral striatum 5 days after UOCCA (Fig. 3 F, F1, K).

In the thalamus, F-J B positive cells were not found in the contralateral thalamus (Fig. 3 G, G1); however, many F-J B positive cells were scattered in the ipsilateral thalamus 5 days after UOCCA (Fig. 3 H, H1, K).

In the hippocampus, no F-J B positive cells were found in the contralateral hippocampus (Fig 3. I-I3). However, abundant F-J B positive cells were sown in the SP of the CA1-3 field of the ipsilateral hippocampus (Fig. 3 J1, J2, K) 5 days after UOCCA. In addition, F-J B positive cells were observed in the GCL and PL of the dentate gyrus in the ipsilateral hippocampus (Fig. 3 J3, K) 5 days after UOCCA.

NeuN immunoreactive neurons

In the contralateral M1 and S1 cortex, NeuN immunoreactive neurons were typically distributed in layers (Fig. 4 A, C). However, in the ipsilateral M1 and S1 cortex, the mean number of NeuN immunoreactive neurons in layers II-III (Fig. 4 B-B2) and V-VI (Fig. 4 D-D2) were significantly decreased by 60.2 % compared to that in the contralateral cortex at 5 days after UOCCA (Fig. 4K).

NeuN immunoreactive neurons in the contralateral striatum were well scattered throughout the striatum (Fig. 4 E, E1). However, NeuN immunoreactive neurons in the ipsilateral striatum were shrunken, and the mean number of NeuN immunoreactive neurons was significantly decreased by 66.2 % compared to those in the contralateral striatum at 5 days after UOCCA (Fig 4 F, F1, K).

In the thalamus, NeuN immunoreactive neurons were easily observed throughout the thalamus of the contralateral side (Fig. 4 G, G1), whereas NeuN immunoreactive neurons in the ipsilateral thalamus were apparently decreased by 71.4% compared to those in the contralateral thalamus at 5 days after UOCCA (Fig. 4 H, H1, K).

In the hippocampus, NeuN immunoreactive neurons in the contralateral side were easily found in the SP of the CA1-3 field (Fig. 4 I1, I2) and in the GCL of the dentate gyrus (Fig. 4 I3). However, the mean number of NeuN immunoreactive neurons in the SP of the CA1 field and CA2/3 field was significantly decreased by 86.8 % and 77.8 %, respectively, compared to that in the contralateral side 5 days after UOCCA (Fig. 4 J1, J2, K). In addition, NeuN immunoreactive neurons in the GCL and PL of the dentate gyrus were decreased by 50.2% and 80.7%, respectively, compared to those in the contralateral side 5 days after UOCCA (Fig. 4 J3, K).

GFAP immunoreactive astrocytes

In the contralateral M1 and S1 cortex, GFAP immunoreactive astrocytes, which had small cell bodies with thin processes,

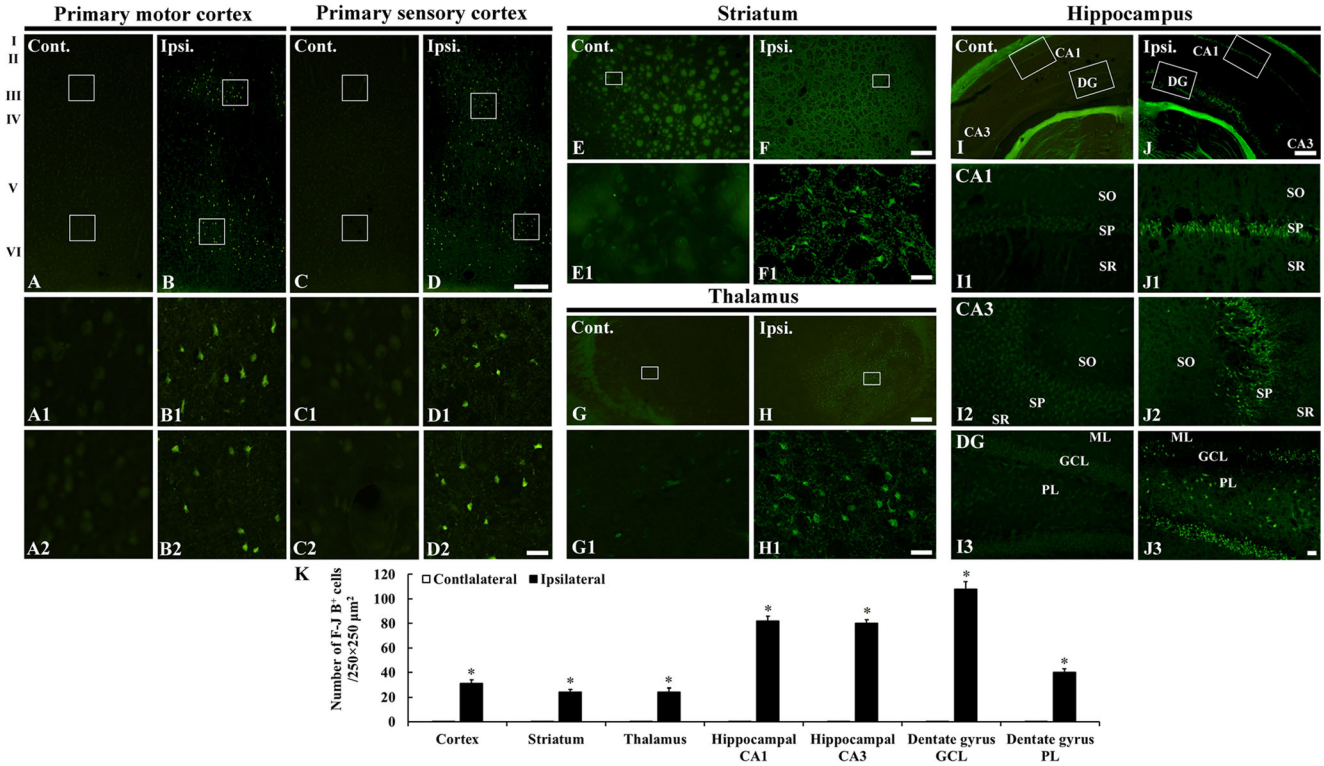

Fig. 3 F-J B histofluorescence staining in the M1 (**a**, **b**) and S1 (**c**, **d**) cortex, striatum (**e**, **f**), thalamus (**g**, **h**), and hippocampus (**i**, **j**) of the contralateral (**a**, **c**, **e**, **g**, **i**) and ipsilateral (**b**, **d**, **f**, **h**, **j**) hemisphere in of the mild group 5 days after UOCCA. In the contralateral M1 and S1 cortex, striatum, thalamus, and hippocampus, no F-J B positive cells are observed. However, in the ipsilateral hemisphere, many F-J B positive cells are shown in layers II-III and V-VI of the M1 and S1 cortex, in the dorsolateral region of the striatum, throughout of the thalamus, in the SP of the CA1-3 filed, and in the GCL and PL of the dentate gyrus. ML, molecular layer; SO, stratum oriens; SR, stratum radiatum. Scale bars: A-J = 200 μm, A1-J3 = 25 μm. K: Number of F-J B positive cells in the cortex, striatum, thalamus, and hippocampus (n = 7; *P<0.05 vs contralateral side). The bars indicate the means ± SEM

were distributed in all cortical layers (Fig. 5 A-A2, C-C2). However, 5 days after UOCCA, GFAP immunoreactive astrocytes became hypertrophied with thickened processes and increased in number by 52.7% in layers II-III (Fig. 5 B-B2) and V-VI (Fig. 5 D-D2) compared to the contralateral M1 and S1 cortex (Fig. 5K).

In the contralateral striatum, GFAP immunoreactive astrocytes were evenly distributed (Fig. 5 E, E1). In the ipsilateral striatum, the number of GFAP immunoreactive astrocyte was significantly decreased by 67.9% compared to that in the contralateral side, and the GFAP immunoreactive astrocytes had dark cell body and swollen processes. (Fig. 5 F, F1, K) 5 days after UOCCA.

In the contralateral thalamus, GFAP immunoreactive astrocytes were scattered throughout the thalamus and they had short processes (Fig. 5 G, G1). GFAP immunoreactive astrocytes in the ipsilateral thalamus became hypertrophied and has long processes, showing that the number of GFAP immunoreactive astrocytes was significantly increased by 78.4% compared to that in the contralateral thalamus 5 days after UOCCA (Fig. 5 H, H1, K).

In the contralateral hippocampus, typical GFAP immunoreactive astrocytes were distributed throughout all layer (Fig. 5 I-I3). In the ipsilateral hippocampus, the distribution of GFAP immunoreactive astrocytes was different according to subregions. In the ipsilateral CA1-3 filed, many of GFAP immunoreactive astrocytes had shrunken cell body with thin processes, and the number of GFAP immunoreactive astrocytes was significantly decreased by 40.4% in the CA1 field and 25.9% in the CA2/3 field, respectively, compared to that in the CA1 and CA2/3 filed 5 days after UOCCA (Fig. 5 J-J2, K). However, GFAP immunoreactive astrocytes in the ipsilateral dentate gyrus showed hypertrophied bulky cytoplasm with thickened processes, and the number of GFAP immunoreactive astrocytes was significantly increased by 81.4% compared to that in the contralateral dentate gyrus (Fig. 5 J3, K).

Iba-1 immunoreactive microglia

In the contralateral M1 and S1 cortex, typical Iba-1 immunoreactive microglia were observed throughout all layers, and they had round cell body with long branched processes (Fig. 6 A-A2, C-C2). However, in the ipsilateral side, Iba-1 immunoreactive microglia became hypertrophied, their processes were swollen and shorten, and a few round Iba-1 immunoreactive microglia were detected (Fig. 6 B, D). In addition, the number

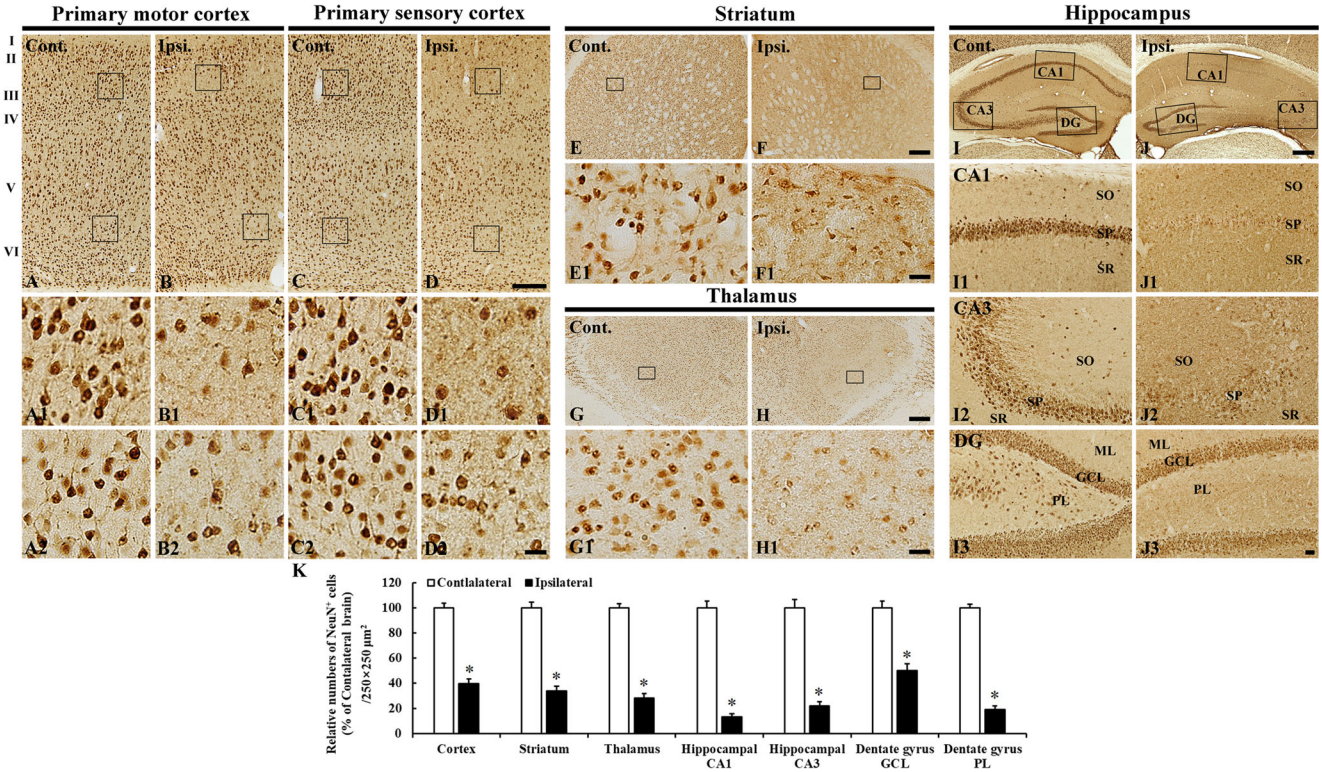

Fig. 4 NeuN immunohistochemistry in the M1 (**a**, **b**) and S1 (**c**, **d**) cortex, striatum (**e**, **f**), thalamus (**g**, **h**), and hippocampus (**i**, **j**) of the contralateral (**a**, **c**, **e**, **g**, **i**) and ipsilateral (**b**, **d**, **f**, **h**, **j**) hemisphere of the mild gerbils 5 days after UOCCA. In the contralateral hemisphere, NeuN immunoreactive neurons are easily observed. In the ipsilateral hemisphere, however, numbers of NeuN immunoreactive neurons in layers II-III and V-VI of the M1 and S1 cortex, in the striatum, and in the thalamus are significantly decreased compared to those in the contralateral side. In the hippocampus, NeuN immunoreactive neurons are distinctively decreased in the SP of the CA1-3 field and in GCL and PL of the dentate gyrus compared to those in the contralateral side. ML, molecular layer; SO, stratum oriens; SR, stratum radiatum. Scale bars: A-J = 200 μm, A1-J3 = 25 μm. K: Relative numbers of NeuN positive cells in the cortex, striatum, thalamus, and hippocampus (n = 7; *P<0.05 vs contralateral side). The bars indicate the means ± SEM

of Iba-1 immunoreactive microglia was significantly increased by 118.6% (Fig. 6 B-B2, 6 D-D2) compared to that in the contralateral side 5 days after UOCCA (Fig. 6K).

In the contralateral striatum, the morphology of Iba-1 immunoreactive microglia was similar to that in the cortex (Fig. 6 E, E1). Cell bodies of Iba-1 immunoreactive microglia in the ipsilateral striatum became hypertrophied, their processes were shortened and swollen, and many of Iba-1 immunoreactive microglia were round in shape (Fig. 6 F, F1). In addition, the number of Iba-1 immunoreactive microglia was significantly increased by 101.8% compared to that in the contralateral striatum 5 days after UOCCA (Fig. 6 K).

In the contralateral thalamus, typical Iba-1 immunoreactive microglia were scattered in the striatum (Fig. 6 G, G1). In the ipsilateral striatum, Iba-1 immunoreactive microglia became distinctly hypertrophied and had branched processes (Fig. 6 H, H1). In addition, the number of them were significantly increased by 168.4% compared to that in the contralateral side 5 days after UOCCA (Fig. 6 K).

In the contralateral hippocampus, typical Iba-1 immunoreactive microglia were distributed throughout all subregions (Fig. 6 I-I3). In the ipsilateral hippocampus, Iba-1 immunoreactive microglia were apparently hypertrophied, and many of Iba-1 positive microglia showed round type (Fig. 6 J-J3). In addition, the number of Iba-1 immunoreactive microglia was significantly increased in all subregions by 159.6% in the CA1-3 filed and 174.1% in the dentate gyrus (Fig. 6 J1, J2, K) and the dentate gyrus by 131.7% (Fig. 6 J3, K) compared to that in the contralateral side 5 days after UOCCA.

Discussions

In the present study, we investigated regional infarcts or selective neuronal death/loss in the ipsilateral hemisphere of the gerbil after 30 min of UOCCA. It has been reported that 30-40% of gerbils results in cerebral infarcts following UOCCA due to their incomplete Willis' circle (Du et al. 2011; Kirino and Sano 1980). In the current study, 43.9% of the gerbils have none-ischemic symptoms, followed by mild symptoms in about 31.8%, moderate symptoms in about 15.2%, and severe symptoms in 9.1% after 30 min of UOCCA. In this study, the severe gerbils died 2-3 days after 30 min of

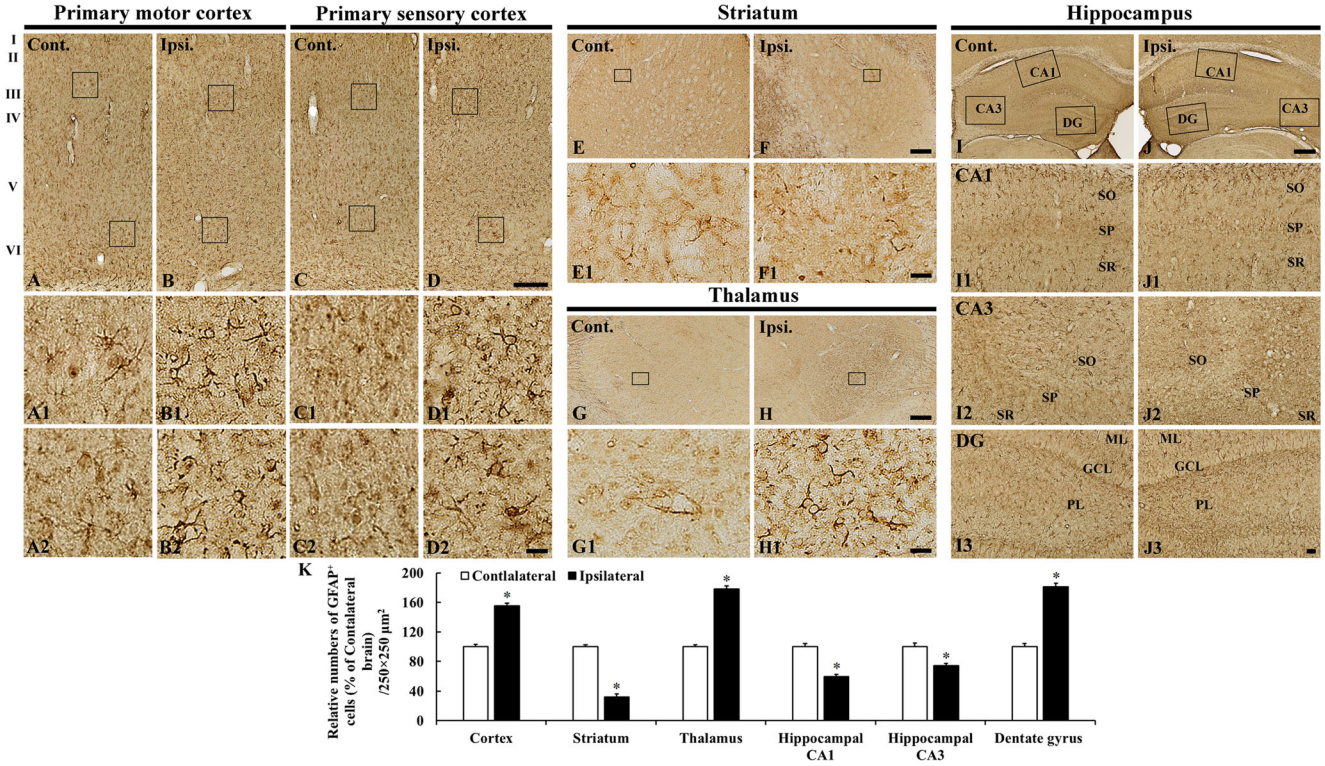

Fig. 5 GFAP immunohistochemistry in the M1 (**a**, **b**) and S1 (**c**, **d**) cortex, striatum (**e**, **f**), thalamus (**g**, **h**), and hippocampus (**i**, **j**) of the contralateral (**a**, **c**, **e**, **g**, **i**) and ipsilateral (**b**, **d**, **f**, **h**, **j**) hemisphere of the mild group 5 days after UOCCA. In the contralateral side, typical GFAP immunoreactive astrocytes are identified. In all the ipsilateral areas, GFAP immunoreactive astrocytes are hypertrophied and increased in number compared to those in the contralateral side. GCL, granular cell layer; ML, molecular layer; PL, polymorphic layer; SO, stratum oriens; SP, stratum pyramidale; SR, stratum radiatum. Scale bars: A-J = 200 μm, A1-J3 = 25 μm. K: Relative numbers of GFAP positive cells in the cortex, striatum, thalamus, and hippocampus (n = 7; *P<0.05 vs contralateral side). The bars indicate the means ± SEM

UOCCA. Based on this finding, we suppose that about 10% of gerbils might die due to absence of the anterior and posterior communication arteries.

Among representative ischemic damages in focal ischemia, necrosis is a form of irreversible tissue injury that neural and non-neural cells, neuropil and blood vessels were all destroyed and results in a tissue dissolution. For example, Baron et al. (2014) reporetd that the severity of ischemic damage in the striatum, which is a main middle cerebral artery (MCA) territory, was infarct (necrosis) after at least 45 min of focal ischemia using MCA occlusion in rats (Baron et al. 2014). On the other hand, it was reported that 20 or 30 min of MCA occlusion resulted in selective neuronal loss/death in the striatum of rats (Momosaki et al. 2017; Park et al. 2018) and mice (Katchanov et al. 2003). In this regard, many studies have used animals with moderate symptoms after transient focal ischemia, therefore, we investigated neuronal damage/loss and gliosis in the moderate infarcts of the gerbils with mild symptom after 30 min of UOCCA, in which model we found a few moderate infarcts in the ipsilateral hemisphere and could conduct the quantification of selective neuronal damage/loss and gliosis (Emmrich et al. 2015).

Selective neuronal loss is defined by death of single neurons showing pyknosis and eosinophilic shrunken cytoplasm along with preserved tissue integrity (Baron et al. 2014; Ishibashi et al. 2004). In addition, selective neuronal loss is observed in non-infarcted penumbra region (at direct periphery of infarct lesion) (Baron et al. 2014; Ejaz et al. 2013). In case of a gerbil model of UOCCA, Kitagawa et al. (1996) reported ischemic cell damage in the hippocampus, caudoputamen, cortex, and thalamus in gerbils with moderate symptom at 7 days after 30 min of UOCCA using hematoxylin-eosin and cresyl violet staining (Kitagawa et al. 1996). Furthermore, Ishibashi et al. (2004) reported that 20 min of UOCCA induced infarcts (necrosis) in the cerebral cortex, striatum, thalamus and hippocampus, showing that a wide range of selective neuronal death was shown by using Klu¨ver-Barrera staining in surrounding infarcts (in penumbra) of moderate symptomatic gerbils 7 days after UOCCA (Ishibashi et al. 2004). Similar to the previous studies, the results of our present study showed that a 30-min episode of UOCCA produced ischemic infarcts (necrosis) stained with TTC in the gerbils with moderate symptoms. Furthermore, we firstly reported that selective neuronal loss was produced in the gerbils with mild symptom in the multiple brain regions including the ipsilateral parietal cortex (in layer II-III and V-VI of the M1 and S1 cortex), the dorsolateral field of the striatum, the thalamus, and the hippocampus at 5 days after UOCCA by

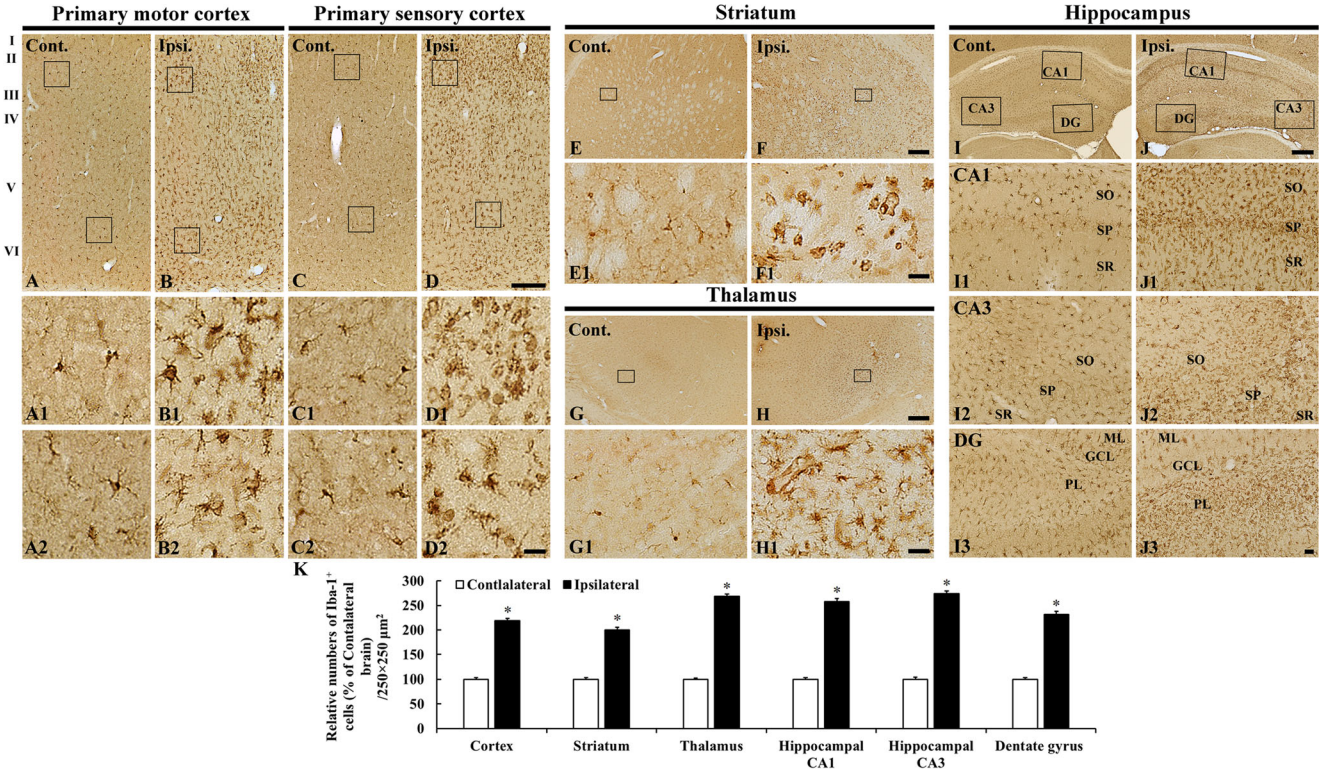

Fig. 6 Iba-1 immunohistochemistry in the M1 (**a**, **b**) and S1 (**c**, **d**) cortex, striatum (**e**, **f**), thalamus (**g**, **h**), and hippocampus (**i**, **j**) of the contralateral (**a**, **c**, **e**, **g**, **i**) and ipsilateral (**b**, **d**, **f**, **h**, **j**) hemisphere of the mild gerbils 5 days after UOCCA. Typical Iba-1 immunoreactive microglia are shown in all the contralateral areas. In all the ipsilateral areas, Iba-1 immunoreactive microglia are hypertrophied and significantly increased in number, in particular, in layers II-III (upper squares; B1, D1) and V-VI (lower squares; B2, D2) of the M1 and S1 cortex, and near the SP of the CA1-3 filed (J1, J2) and in the PL of the dentate gyrus (J3). GCL, granular cell layer; ML, molecular layer; PL, polymorphic layer; SO, stratum oriens; SP, stratum pyramidale; SR, stratum radiatum. Scale bars: A-J = 200 μm, A1-J3 = 25 μm. K: Relative numbers of Iba-1 positive cells in the cortex, striatum, thalamus, and hippocampus (n = 7; *P<0.05 vs contralateral side). The bars indicate the means ± SEM

using F-J B fluorescence staining, which clearly detects degenerating/dead neurons (Schmued and Hopkins 2000). In particular, we firstly found obvious neuronal death/degeneration of pyramidal cells in the hippocampal CA3 area and granule cells in the dentate gyrus at 5 days after UOCCA, which have been known as the most tolerant (relatively resistant) cells to transient ischemic insults (Pulsinelli 1985). As to ischemic damage of CA3 pyramidal neurons and dentate granule cells following after transient ischemia, we recently reported that CA3 pyramidal neurons and dentate granule cells were dead in the gerbil hippocampus after 5 min of transient ischemia under hyperthermia (39 ± 0.5°C) (Kim et al. 2015). It has been reported that multiple infarctions in gerbils after repetitive obstruction of carotid arteries or chronic low perfusion resulted in persistent cognitive impairments similar to symptoms of multi-infarct dementia in a clinical setting (Naritomi 1991). Taken together, our present results indicate that 30 min of UOCCA could develop selective neuronal death of multiple brain regions even less vulnerable cells (pyramidal cells in the primary motor cortex, CA3 pyramidal and dentate granule cells) in the ipsilateral hemisphere of the gerbils with mild symptoms. Further studies on chronological changes in their selective neuronal death in the ipsilateral hemisphere after 30 min of UOCCA need to confirm when selective neuronal death starts. In addition, cognitive and behavioral studies in this gerbil model of UOCCA will be helpful in studying restorative processes in chronic phase after stroke.

In this study, we demonstrated GFAP and Iba-1 expressions in astrocytes and microglia, respectively, reacting in the ipsilateral hemisphere of the mild symptomatic gerbils induced by 30 min of UOCCA by using immunohistochemistry for GFAP and Iba-1. First, in the ipsilateral hemisphere, interestingly, the majority of astrocytes stained with GFAP were reduced in number in the dorsolateral field of the striatum and hippocampal CA1-3 regions, while strong GFAP expressions in reactive astrocytes were markedly increased in the M1 and S1 cortex, thalamus, and dentate gyrus at 5 days after UOCCA. Matsui et al. (2002) reported chronologic patterns of GFAP expression as follows: reactive astrocytes were strongly stained with GFAP at 3-4 days after ischemia, showing that numbers of GFAP positive reactive astrocytes were apparently decreased in the periinfarct area, where selective neuronal death was observed, at 7 days after permeant MCA occlusion (Matsui et al. 2002). Furthermore, Ouyang et al. (2007) reported regional astrocyte vulnerability based on reduced GFAP immunoreactivity in the rat hippocampus

after transient forebrain ischemia as follows: astrocytes in the CA1 filed were more sensitive to ischemia than astrocytes in the dentate gyrus, and the selective astrocytic dysfunction was closely related to neuronal damage in the CA1 filed and dentate gyrus after transient forebrain ischemia (Ouyang et al. 2007). Taken together, it is likely that regional expression pattern of GFAP, an astrocyte-specific intermediate filament protein, in astrocytes is different depending on post ischemic period, and the regional difference in astrocyte impairment maybe closely related to severity of ischemic neuronal damage in the ipsilateral hemisphere after 30 min of UOCCA.

On top of that, in the present study, morphologically activated Iba-1 immunoreactive microglia and round type Iba-1 immunoreactive cells appeared, showing that numbers of Iba-1 immunoreactive microglia were significantly increased in the cortex, striatum, thalamus, and hippocampus of the ipsilateral hemisphere, where ischemic neuronal death was found at 5 days after UOCCA. It has been reported that the activation of microglia as well as astrocytes induced by mild focal ischemia precedes selective neuronal death: this phenomenon may be an important factor in selective neuronal death (Ejaz et al. 2013; Miyajima et al. 2018). Furthermore, activations of microglia and astrocytes are still characterized after prolonged periods (28 days) in selective neuronal death areas following brief focal ischemia (Baron et al. 2014; Emmrich et al. 2015). As to their activation, it has been demonstrated that cerebral ischemia/reperfusion activates the immune system in the brain, and astrocytes and microglia response to ischemia to play essential roles in inflammation and tissue repair (Barakat and Redzic 2016; Choudhury and Ding 2016; Kim et al. 2016). Based on the previous studies with our present findings, our present data imply a high association of enhanced Iba-1 and GFAP expressions in the ipsilateral hemisphere with occurrence of selective neuronal death.

To sum up, this study reveals that 30 min of UOCCA induced infarcts or selective neuronal death in the ipsilateral M1 and S1 cortex, striatum, thalamus, and hippocampus depending on severity of ischemic symptoms in gerbils at 5 days after 30 min of UOCCA. In addition, selective neuronal death/loss was induced in the above described regions of mild symptomatic gerbils, and a substantial degree of activated astrocytes and microglia were found, although numbers of GFAP and/or Iba-1 immunoreactive cells were different depending on the ischemic regions 5 days after UOCCA.

Acknowledgements This research was supported by the Bio & Medical Technology Development Program of the NRF funded by the Korean government, MSIP (NRF-2015M3A9B6066835), by 2017 Research Grant from Kangwon National University (No. 520170438), by "Cooperative Research Program for Agriculture Science and Technology Development (Project No. PJ01329401)" Rural Development Administration, Republic of Korea, and by Cooperative Research Program for Agriculture Science and Technology Development (Project No. PJ01321101)" Rural Development Administration, Republic of Korea.

Compliance with ethical standards

The experimental protocol of this study was approved by the Institutional Animal Care and Use Committee (IACUC) at Kangwon National University (approval no. KW-180124-1) and is in accordance with the guidelines following current international laws and policies (NIH Guide for the Care and Use of Laboratory Animals, The National Academies Press, 8th Ed., 2011).

Conflict of Interest The authors declare that they have no conflict of interest.

References

Ahn JH, Shin BN, Park JH et al (2016) Long-term observation of neuronal degeneration and microgliosis in the gerbil dentate gyrus after transient cerebral ischemia. J Neurol Sci 363:21–26

Bae EJ, Chen BH, Shin BN et al (2015) Comparison of immunoreactivities of calbindin-D28k, calretinin and parvalbumin in the striatum between young, adult and aged mice, rats and gerbils. Neurochem Res 40:864–872

Barakat R, Redzic Z (2016) The Role of Activated Microglia and Resident Macrophages in the Neurovascular Unit during Cerebral Ischemia: Is the Jury Still Out? Med Princ Pract 25(Suppl 1):3–14

Baron JC, Yamauchi H, Fujioka M, Endres M (2014) Selective neuronal loss in ischemic stroke and cerebrovascular disease. J Cereb Blood Flow Metab 34:2–18

Canazza A, Minati L, Boffano C, Parati E, Binks S (2014) Experimental models of brain ischemia: a review of techniques, magnetic resonance imaging, and investigational cell-based therapies. Front Neurol 5:19

Candelario-Jalil E, Alvarez D, Merino N, Leon OS (2003) Delayed treatment with nimesulide reduces measures of oxidative stress following global ischemic brain injury in gerbils. Neurosci Res 47:245–253

Choudhury GR, Ding S (2016) Reactive astrocytes and therapeutic potential in focal ischemic stroke. Neurobiol Dis 85:234–244

Du XY, Zhu XD, Dong G et al (2011) Characteristics of circle of Willis variations in the mongolian gerbil and a newly established ischemia-prone gerbil group. ILAR J 52:E1–E7

Ejaz S, Williamson DJ, Ahmed T et al (2013) Characterizing infarction and selective neuronal loss following temporary focal cerebral ischemia in the rat: a multi-modality imaging study. Neurobiol Dis 51:120–132

Emmrich JV, Ejaz S, Neher JJ, Williamson DJ, Baron JC (2015) Regional distribution of selective neuronal loss and microglial activation across the MCA territory after transient focal ischemia: quantitative versus semiquantitative systematic immunohistochemical assessment. J Cereb Blood Flow Metab 35:20–27

Ha Park J, Yoo KY, Hye Kim I et al (2016) Hydroquinone Strongly Alleviates Focal Ischemic Brain Injury via Blockage of Blood-Brain Barrier Disruption in Rats. Toxicol Sci 154:430–441

Hanyu S, Ito U, Hakamata Y, Yoshida M (1993) Repeated unilateral carotid occlusion in Mongolian gerbils: quantitative analysis of cortical neuronal loss. Acta Neuropathol 86:16–20

Hanyu S, Ito U, Hakamata Y, Yoshida M (1995) Transition from ischemic neuronal necrosis to infarction in repeated ischemia. Brain Res 686:44–48

Hanyu S, Ito U, Hakamata Y, Nakano I (1997) Topographical analysis of cortical neuronal loss associated with disseminated selective neuronal necrosis and infarction after repeated ischemia. Brain Res 767:154–157

Ishibashi S, Kuroiwa T, Endo S, Okeda R, Mizusawa H (2003) Neurological dysfunctions versus regional infarction volume after focal ischemia in Mongolian gerbils. Stroke 34:1501–1506

Ishibashi S, Kuroiwa T, Katsumata N, Yuan S, Endo S, Mizusawa H (2004) Extrapyramidal motor symptoms versus striatal infarction volume after focal ischemia in mongolian gerbils. Neuroscience 127:269–275

Ito U, Hakamata Y, Watabe K, Oyanagi K (2014) Mannitol infusion immediately after reperfusion suppresses the development of focal cortical infarction after temporary cerebral ischemia in gerbils. Neuropathology 34:360–369

Katchanov J, Waeber C, Gertz K et al (2003) Selective neuronal vulnerability following mild focal brain ischemia in the mouse. Brain Pathol 13:452–464

Kim DW, Cho JH, Cho GS et al (2015) Hyperthermic preconditioning severely accelerates neuronal damage in the gerbil ischemic hippocampal dentate gyrus via decreasing SODs expressions. J Neurol Sci 358:266–275

Kim JY, Park J, Chang JY, Kim SH, Lee JE (2016) Inflammation after Ischemic Stroke: The Role of Leukocytes and Glial Cells. Exp Neurobiol 25:241–251

Kirino T, Sano K (1980) Changes in the contralateral dentate gyrus in Mongolian gerbils subjected to unilateral cerebral ischemia. Acta Neuropathol 50:121–129

Kirino T, Sano K (1984) Selective vulnerability in the gerbil hippocampus following transient ischemia. Acta Neuropathol 62:201–208

Kitagawa K, Matsumoto M, Matsushita K et al (1996) Ischemic tolerance in moderately symptomatic gerbils after unilateral carotid occlusion. Brain Res 716:39–46

Lee JC, Ahn JH, Lee DH et al (2013) Neuronal damage and gliosis in the somatosensory cortex induced by various durations of transient cerebral ischemia in gerbils. Brain Res 1510:78–88

Lee JC, Park JH, Ahn JH et al (2016a) New GABAergic Neurogenesis in the Hippocampal CA1 Region of a Gerbil Model of Long-Term Survival after Transient Cerebral Ischemic Injury. Brain Pathol 26: 581–592

Lee TK, Park JH, Ahn JH et al (2016b) Pretreated duloxetine protects hippocampal CA1 pyramidal neurons from ischemia-reperfusion injury through decreases of glial activation and oxidative stress. J Neurol Sci 370:229–236

Levy DE, Brierley JB, Plum F (1975) Ischaemic brain damage in the gerbil in the absence of'no-reflow'. J Neurol Neurosurg Psychiatry 38:1197–1205

Matsui T, Mori T, Tateishi N et al (2002) Astrocytic activation and delayed infarct expansion after permanent focal ischemia in rats. Part I: enhanced astrocytic synthesis of S-100β in the periinfarct area precedes delayed infarct expansion. J Cereb Blood Flow Metab 22: 711–722

Matsumoto M, Hatakeyama T, Akai F, Brengman JM, Yanagihara T (1988) Prediction of stroke before and after unilateral occlusion of the common carotid artery in gerbils. Stroke 19:490–497

Miyajima N, Ito M, Rokugawa T et al (2018) Detection of neuroinflammation before selective neuronal loss appearance after mild focal ischemia using [(18)F]DPA-714 imaging. EJNMMI Res 8:43

Momosaki S, Ito M, Yamato H et al (2017) Longitudinal imaging of the availability of dopamine transporter and D2 receptor in rat striatum following mild ischemia. J Cereb Blood Flow Metab 37:605–613

Murakami K, Kondo T, Kawase M, Chan PH (1998) The development of a new mouse model of global ischemia: focus on the relationships between ischemia duration, anesthesia, cerebral vasculature, and neuronal injury following global ischemia in mice. Brain Res 780: 304–310

Naritomi H (1991) Experimental basis of multi-infarct dementia: memory impairments in rodent models of ischemia. Alzheimer Dis Assoc Disord 5:103–111

Ohno K, Ito U, Inaba Y (1984) Regional cerebral blood flow and stroke index after left carotid artery ligation in the conscious gerbil. Brain Res 297:151–157

Oostveen JA, Timby K, Williams LR (1992) Prediction of cerebral ischemia by ophthalmoscopy after carotid occlusion in gerbils. Stroke 23: 1588–1593

Ouyang YB, Voloboueva LA, Xu LJ, Giffard RG (2007) Selective dysfunction of hippocampal CA1 astrocytes contributes to delayed neuronal damage after transient forebrain ischemia. J Neurosci 27: 4253–4260

Park JH, Cho JH, Ahn JH et al (2018) Neuronal loss and gliosis in the rat striatum subjected to 15 and 30 minutes of middle cerebral artery occlusion. Meta Brain Dis 33:775–784

Pulsinelli WA (1985) Selective neuronal vulnerability: morphological and molecular characteristics. Prog Brain Res 63:29–37

Radtke-Schuller S, Schuller G, Angenstein F, Grosser OS, Goldschmidt J, Budinger E (2016) Brain atlas of the Mongolian gerbil (Meriones unguiculatus) in CT/MRI-aided stereotaxic coordinates. Brain Struct Funct 221(Suppl 1):1–272

Rodriguez Cruz Y, Mengana Tamos Y, Munoz Cernuda A et al (2010) Treatment with nasal neuro-EPO improves the neurological, cognitive, and histological state in a gerbil model of focal ischemia. TheScientificWorldJournal 10:2288–2300

Schmued LC, Hopkins KJ (2000) Fluoro-Jade B: a high affinity fluorescent marker for the localization of neuronal degeneration. Brain Res 874:123–130

Schmued LC, Albertson C, Slikker W Jr (1997) Fluoro-Jade: a novel fluorochrome for the sensitive and reliable histochemical localization of neuronal degeneration. Brain Res 751:37–46

Sicard KM, Fisher M (2009) Animal models of focal brain ischemia. Exp Transl Stroke Med 1:7